Journal of
Mechanics of
Materials and Structures

# THE HEMISPHERICAL NANOPIT AT THE PLANE BOUNDARY OF AN ELASTIC HALF-SPACE SUBJECTED TO STATICALLY EQUIVALENT SHEAR TRACTIONS

Changwen Mi, Zhongwei Sun and Demitris Kouris

Volume 11, No. 5 December 2016

msp

JOURNAL OF MECHANICS OF MATERIALS AND STRUCTURES
Vol. 11, No. 5, 2016
dx.doi.org/10.2140/jomms.2016.11.595

msp

# THE HEMISPHERICAL NANOPIT AT THE PLANE BOUNDARY OF AN ELASTIC HALF-SPACE SUBJECTED TO STATICALLY EQUIVALENT SHEAR TRACTIONS

CHANGWEN MI, ZHONGWEI SUN AND DEMITRIS KOURIS

The elastic deformation of a semi-infinite substrate containing a nanosized hemispherical pit on its plane boundary crucially relies on the mechanical response of the pit surface. In this paper, we develop a micromechanical model that couples Gurtin and Murdoch's model of surface mechanics with the classical theory of elasticity, and we explicitly evaluate the stress concentration, displacement and stress distribution resulting from a family of statically equivalent shear tractions applied on the pit surface. We found that two intrinsic dimensionless parameters, both constructed from the characteristic length and material properties, govern the highly localized elastic field. Both the magnitude and sign of these parameters are of great importance. Negative values tend to increase stress concentrations, whereas positive ones have the opposite effect. We further highlight the consequences of our analysis by comparing a number of shear tractions that correspond to the same torque. The comparison provides the means of evaluating the degree of difference in elastic fields in the immediate vicinity of statically equivalent force distributions.

## 1. Introduction

The discontinuities in geometry and load distribution are primary causes of stress concentrations that affect the otherwise smooth stress variations in elastic solids. The presence of geometric defects and concentrated loads typically results in high stresses that are multiple times greater than their nominal values in small and localized regions [Barber 2010]. Experimental methods and advanced theoretical and numerical analysis are means of determining stress concentrations. Many results of practical engineering importance can be found in the literature [Young and Budynas 2002].

Nevertheless, recent advancements in surface/interface mechanics call for a reevaluation of stress concentrations near geometric defects at the nanoscale [Wang et al. 2011]. It is a fact that the area-to-volume ratio of an elastic element is inversely proportional to its characteristic length [Sharma et al. 2003; Mi and Kouris 2014b]. The order of magnitude of this ratio can be as large as nine as the relevant characteristic length goes from the macroscopic level down to the nanoscale. At such a small length scale, the contribution of surface strain energy becomes comparable or even dominant to that of its bulk counterpart in the total strain energy stored in the system [Streitz et al. 1994; Wang et al. 2011]. The linearly elastic model specifically tailored for a coherent surface/interface proposed by Gurtin and Murdoch [1975; 1978] has gained major popularity in a continuous effort to couple surface effects with the classical theory of elasticity [Sharma et al. 2003; Mi and Kouris 2006; 2014a; 2014b; He and Li 2006; Kushch et al. 2013; Steigmann and Ogden 1999]. Closed-form, semianalytical and numerical solutions have all been developed to investigate the consequences of material surface/interface on both

*Keywords:* surface mechanics, nanopit, half-space, torsional loading, stress concentration.

the overall effective modulus and the localized elastic field [Wang et al. 2011]. Among these works, stress concentration near geometric defects at the nanoscale is one of the most important foci [He and Li 2006; Mi and Kouris 2013].

Theoretical analysis performed within the context of Gurtin–Murdoch's surface mechanics model and the classical theory of elasticity shows that the introduction of surface effects inevitably calls for a modification to the solution predicted by the classical theory of elasticity alone. The net effect is dependent on the type of surface model and the material properties describing the mechanical behavior of a solid surface. For example, for a spherical nanocavity embedded in an infinite or semi-infinite elastic, substrate positive surface material parameters tend to alleviate the stress concentration effect, in the case of a metal surface [He and Li 2006; Mi and Kouris 2013; 2015]. This argument is supported by molecular dynamics simulations of a spherical cavity inside an aluminum substrate axially loaded at a high strain rate [Mi et al. 2011]. It can also be expected that the inclusion of a surface mechanics model worsens the stress concentration, provided that the sign of surface materials properties is reversed.

While previous studies focus on the stress concentration behavior near a nanoscale geometric defect subjected merely to nontorsional loads, the present work is directed towards the investigation of stress concentrations under torsional deformation modes. When a twisting moment is transmitted through a rigid-sphere embedded in an elastic medium, shear tractions develop on the surface of the rigid inclusion [Hill 1966; Miyao et al. 1975]. In geotechnical engineering, both the static and dynamic behaviors of rigid inclusions provide practical means of exploring the response of infrastructure foundations resting in soil environments [Kausel 2010; Osman and Rouainia 2012]. Rigid inclusions also find applications in offshore engineering, where vessels and floating structures are supported by anchors of different shapes. In large scale systems, attention is typically paid to the dynamic propagation of elastic waves generated by programming the motion of a distant rigid sphere or by applying dynamic loads on the surface of a distant void. Stress distributions in the vicinity of the rigid sphere or cavity are another concern [Eringen 1957]. Torsion is one of the most important loading conditions considered in the literature [Reissner and Sagoci 1944; Williams 1971; Chadwick and Johnson 1971; Zakout et al. 1999].

The behavior of these solutions due to a rigid sphere or void at the nanoscale is intricate and requires further consideration. These problems naturally arise in nanoelectromechanical systems, particularly in those systems involving structural elements made from soft materials. Since both the bulk and surface material properties of soft materials are several orders of magnitude lower than those of metals [Gere and Goodno 2009; Markidou et al. 2005; Białopiotrowicz and Jańczuk 2002; Weijs et al. 2014], particles of secondary phases easily serve as rigid inclusions. In this case, torsional loading naturally kicks in, due to the strong resistance of rigid particles to both volume and shape changes. As an early attempt to reach this goal, here we consider a nanosized hemispherical pit at the plane boundary of an elastic half-space subjected to a family of statically equivalent shear tractions.

The static equivalence means that the first moment of any traction mode with respect to the $z$-axis reduces to the same torque. The effects of the pit surface were modeled by the coherent surface model of Gurtin and Murdoch. This model consists of three components: a definition of surface strain, a surface constitutive relation, and a force-balance law, as detailed in the original article [Gurtin and Murdoch 1978] as well as in the main body of the present paper. The method of displacement potential renders us an efficient solution strategy for a three-dimensional torsional problem like the one we are examining [Barber 2010]. A single Boussinesq displacement potential function represented by an infinite series is sufficient

to yield the required solution that satisfies a given shear traction boundary condition. The obtained solution converges rapidly as a function of the number of terms included in the series and is available in closed-form for certain forms of shear tractions. This approach is capable of generating displacements and stresses at any point in the pitted half-space, including the stress concentration conditions at the pit surface.

We show that the resultant elastic field is extremely localized and is dependent upon to two key intrinsic dimensionless parameters that are constructed from the pit radius, shear modulus of the half-space, and the residual surface tension and shear modulus of the pit surface. The surface material parameter that represents the dilatational deformation of an area element turns out to be irrelevant to twisting deformation. Depending on both the magnitude and sign of the two intrinsic dimensionless parameters, the pit surface model could alleviate or aggravate the stress concentration and distribution to a certain extent. Dimension analysis suggests that the pit surface effects are much more significant for a soft solid than for a metal material. In addition, by comparing different modes of shear tractions resulting in the exact same torque, the developed solution provided us a means of examining the degree of difference in elastic stresses near statically equivalent force distributions.

In Section 2, we derive a micromechanical model to determine the displacements and stresses in the half-space, which we use to derive both closed-form and semianalytical solutions in Section 3. The causes and consequences of these solutions will also be discussed in detail in this section. Finally, in Section 4, we discuss a number of conclusions drawn from the theoretical and numerical analysis.

## 2. Method of solution

We consider a hemispherical pit of radius $a$, centered at the free surface of a semi-infinite elastic solid, as shown in Figure 1. The center of the pit was chosen as the common origin for the cylindrical $(r, \theta, z)$ and spherical $(R, \varphi, \theta)$ coordinates. The elastic half-space is modeled as an isotropic and linearly elastic material with shear modulus $G$ and Poisson's ratio $\nu$. The external loading is modeled by a family of statically equivalent shear tractions applied on the hemispherical pit surface. The net moment of these shear tractions with respect to the symmetry axis $z$ corresponds to the exact same torque $T$. The mechanical property of the pit surface is characterized by the residual surface stress $\tau_0$ and two surface Lamé constants $\lambda_0$ and $\mu_0$.

The method of displacement potentials was adopted to tackle the present problem. For the case of axial symmetric torsion in the absence of body forces, a single harmonic function (e.g., $\lambda_3$) is sufficient to represent the solution. This harmonic function is part of the well known Boussinesq displacement potentials that was first proposed by Boussinesq in his memoirs in 1888, and later quoted by Todhunter and Pearson [2010]. The harmonic function $\lambda_3$ automatically satisfies the elastostatic Navier's equation

$$\nabla^2 \boldsymbol{u} + \frac{1}{1-2\nu} \nabla(\nabla \cdot \boldsymbol{u}) = \boldsymbol{0}, \tag{1}$$

via the representation $2G\boldsymbol{u} = \nabla \times (\boldsymbol{k}\lambda_3)$, where $\boldsymbol{u}$ is the displacement vector and $\boldsymbol{k}$ denotes a unit vector oriented in the $z$-direction. The displacement potential $\lambda_3$ could be related to the more familiar Papkovich–Neuber solution to the equilibrium equation of displacements (1) via [Barber 2010]

$$\phi = -\frac{1}{4(1-\nu)} \nabla \times (\boldsymbol{k}\lambda_3). \tag{2}$$

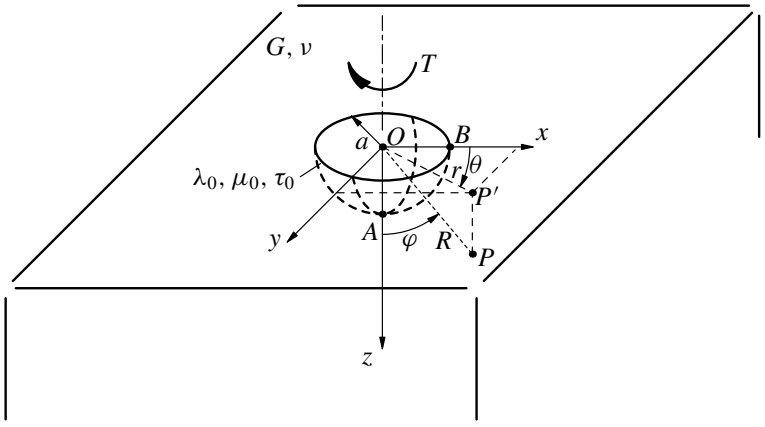


**Figure 1.** Geometry of the problem.

In terms of spherical coordinates, the displacements resulting from the single torsional potential $\lambda_3$ read

$$2Gu_R = \frac{1}{R}\frac{\partial \lambda_3}{\partial \theta}, \quad 2Gu_\varphi = \frac{\cot\varphi}{R}\frac{\partial \lambda_3}{\partial \theta}, \quad 2Gu_\theta = -\frac{\cos\varphi}{R}\frac{\partial \lambda_3}{\partial \varphi} - \sin\varphi\frac{\partial \lambda_3}{\partial R}. \tag{3}$$

The change of variable $\mu = \cos[\varphi]$ transforms the displacement components into

$$2Gu_R = \frac{1}{R}\frac{\partial \lambda_3}{\partial \theta}, \quad 2Gu_\varphi = \frac{\mu}{R\sqrt{1-\mu^2}}\frac{\partial \lambda_3}{\partial \theta}, \quad 2Gu_\theta = \sqrt{1-\mu^2}\left(\frac{\mu}{R}\frac{\partial \lambda_3}{\partial \mu} - \frac{\partial \lambda_3}{\partial R}\right). \tag{4}$$

Recall that under the condition of axial symmetry, all derivatives with respect to $\theta$ vanish and hence

$$u_R = u_\varphi = 0, \quad 2Gu_\theta = \sqrt{1-\mu^2}\left(\frac{\mu}{R}\frac{\partial \lambda_3}{\partial \mu} - \frac{\partial \lambda_3}{\partial R}\right). \tag{5}$$

The corresponding stress components are then given by

$$\begin{gathered}
\sigma_{RR} = \sigma_{\varphi\varphi} = \sigma_{\theta\theta} = \sigma_{R\varphi} = 0, \\
\frac{\sigma_{R\theta}}{\sqrt{1-\mu^2}} = \frac{1}{2R}\frac{\partial \lambda_3}{\partial R} - \frac{1}{2}\frac{\partial^2 \lambda_3}{\partial R^2} + \frac{1}{2R^2(1-\mu^2)}\frac{\partial^2 \lambda_3}{\partial \theta^2} - \frac{\mu}{R^2}\frac{\partial \lambda_3}{\partial \mu} + \frac{\mu}{2R}\frac{\partial^2 \lambda_3}{\partial R \partial \mu}, \\
\sigma_{\varphi\theta} = \frac{\mu}{R}\frac{\partial \lambda_3}{\partial R} + \frac{\mu}{2}\frac{\partial^2 \lambda_3}{\partial R^2} - \frac{(1+\mu^2)}{2R^2}\frac{\partial \lambda_3}{\partial \mu} + \frac{(1-\mu^2)}{2R}\frac{\partial^2 \lambda_3}{\partial R \partial \mu}.
\end{gathered} \tag{6}$$

Since $P_n[\cos\varphi]/R^{n+1}$, where $P_n$ is the Legendre polynomial with the argument $\mu = \cos[\varphi]$, is a spherical harmonic function for an arbitrary integer $n$ [Arfken and Weber 2013], a more general representation can be written in the form

$$\lambda_3 = G\sum_{n=0}^{\infty} A_n \frac{a^{2n+3}}{R^{2n+1}} P_{2n}[\mu], \tag{7}$$

where $A_n$ stands for the unknown coefficients to be determined from the boundary conditions. The shear modulus and power function of the pit radius were introduced to make the unknown coefficients dimensionless. It should also be noted that in this representation only even orders of Legendre polynomials were incorporated in order to clear tractions at the straight boundary of the pitted half-space.

Upon substituting the potential function (7) into (5) and (6), the nonzero displacement and stress components become

$$2Gu_\theta = G\sqrt{1-\mu^2}\sum_{n=0}^{\infty}\left\{A_n\frac{a^{2n+3}}{R^{2n+2}}\big((2n+1)P_{2n}[\mu]+\mu P'_{2n}[\mu]\big)\right\}, \tag{8}$$

$$\begin{aligned}\sigma_{R\theta} &= -\tfrac{1}{2}G\sqrt{1-\mu^2}\sum_{n=0}^{\infty}\left\{A_n\frac{a^{2n+3}}{R^{2n+3}}(2n+3)\big((2n+1)P_{2n}[\mu]+\mu P'_{2n}[\mu]\big)\right\},\\ \sigma_{\varphi\theta} &= -\frac{(1-\mu^2)}{2}G\sum_{n=1}^{\infty}A_n\frac{a^{2n+3}}{R^{2n+3}}\big\{(2n+2)P'_{2n}[\mu]+\mu P''_{2n}[\mu]\big\}.\end{aligned} \tag{9}$$

The above expressions can be simplified to

$$2Gu_\theta = -G\sum_{n=0}^{\infty}\left\{A_n\frac{a^{2n+3}}{R^{2n+2}}P^1_{2n+1}[\mu]\right\}, \tag{10}$$

$$\sigma_{R\theta} = \tfrac{1}{2}G\sum_{n=0}^{\infty}\left\{A_n\frac{a^{2n+3}}{R^{2n+3}}(2n+3)P^1_{2n+1}[\mu]\right\}, \quad \sigma_{\varphi\theta} = -\tfrac{1}{2}G\sum_{n=1}^{\infty}\left\{A_n\frac{a^{2n+3}}{R^{2n+3}}P^2_{2n+1}[\mu]\right\}. \tag{11}$$

by the introduction of the recurrence relation of Legendre polynomials [Arfken and Weber 2013]

$$P'_{2n+1}[\mu] = (2n+1)P_{2n}[\mu]+\mu P'_{2n}[\mu], \tag{12}$$

and the associated Legendre function of the first kind [loc. cit.]

$$P^m_n[\mu] = (-1)^m(1-\mu^2)^{m/2}\frac{\mathrm{d}^m}{\mathrm{d}\mu^m}P_n[\mu]. \tag{13}$$

At the straight boundary of the half-space, as illustrated by (6) and (11),

$$\sigma_{\varphi R} = \sigma_{\varphi\varphi} = 0, \quad \sigma_{\varphi\theta} = -\tfrac{1}{2}\sum_{n=1}^{\infty}\left\{A_n\frac{a^{2n+3}}{R^{2n+3}}P^2_{2n+1}[0]\right\}. \tag{14}$$

The parity relation satisfied by the associated Legendre functions exemplifies that $P^m_n[\mu]$ is an odd function provided that $n+m$ is an odd number [Arfken and Weber 2013]. As a result, the only nonzero stress component $\sigma_{\varphi\theta}$ also disappears on the straight boundary of the half-space $\mu = 0$.

As one of the most adopted models of surface mechanics, Gurtin and Murdoch [1975] chose to treat a solid surface as an elastic layer of material boundary whose thickness is vanishingly small. Within the context of their theory, the fundamental equations that govern the mechanical behavior of the pit surface (i.e., the surface version of the displacement-strain relation, surface constitutive law and force

equilibrium condition) can be formulated as [Gurtin and Murdoch 1978]

$$\mathrm{E}_{\alpha\beta} = \tfrac{1}{2}((\nabla_{\mathrm{S}}\boldsymbol{u})_{\alpha\beta} + (\nabla_{\mathrm{S}}\boldsymbol{u})_{\beta\alpha}), \tag{15}$$

$$\Sigma_{\alpha\beta} = \tau_0\delta_{\alpha\beta} + 2(\mu_0 - \tau_0)\mathrm{E}_{\alpha\beta} + (\lambda_0 + \tau_0)\mathrm{E}_{\gamma\gamma}\delta_{\alpha\beta} + \tau_0\langle\nabla_{\mathrm{S}}\boldsymbol{u}\rangle_{\alpha\beta}, \quad \Sigma_{3\alpha} = \tau_0\langle\nabla_{\mathrm{S}}\boldsymbol{u}\rangle_{3\alpha}, \tag{16}$$

$$\sigma_{ij}n_j = (\nabla_{\mathrm{S}}\cdot\Sigma)_i + T_i^{(\boldsymbol{n})}, \tag{17}$$

where E stands for the $2\times 2$ surface strain tensor defined on the hemispherical pit surface with unit normal vector $\boldsymbol{n} = -\boldsymbol{e}_R$. Its four components are the same as the corresponding ones in the bulk strain tensor when confined to the pit surface. In contrast, the surface stress tensor $\Sigma$ is defined as a $3\times 2$ superficial tensor, i.e., only those three of its nine components applied perpendicular to the pit surface were not taken into account [Mogilevskaya et al. 2010]. As a result, the surface stress tensor is not a symmetric one, a well known property possessed by its bulk counterpart. To completely describe the mechanical response of the pit surface, three surface moduli ($\tau_0$, $\lambda_0$ and $\mu_0$) are required.

Particularly, the first term in the right hand side of the first equation of (16) states that the two normal components $\Sigma_{11}$ and $\Sigma_{22}$ do not vanish in the absence of external loads. Namely, this term is deformation-independent. Nonetheless, if we decompose the work done by the surface stress tensor against the surface strain field, the contribution due to this term will only enter into the resultant area component but not the distorsional one. Consequently, this deformation-independent term is not compatible with the torsional deformation considered in the present work. Its effects should be studied in terms of loading conditions that result in area/volume changes [He and Li 2006; Mogilevskaya et al. 2008; Mi and Kouris 2013].

It is also worth mentioning that the net traction at the pit surface does not vanish — in contrast, it must be balanced by the surface divergence of the surface stress. Equation (17) directly bridges the gap between surface mechanics and the classical bulk elasticity.

The above unique properties of a solid material surface serve as a fundamental tool for understanding the various counter-classical phenomena that have been observed in nanoscale materials and structures. The finite curvature of radius $a$ of the hemispherical pit surface suggests that its surface mechanics effects are of primary importance when compared to those of the half-space straight boundary. As a result, we have chosen not to account for the latter in the present work.

In (15) and (16), the explicit expressions of the surface gradient of displacements should be self-explanatory in Cartesian coordinates. In spherical coordinates, however, unit coordinate vectors ($\boldsymbol{e}_R$, $\boldsymbol{e}_\varphi$, $\boldsymbol{e}_\theta$) are themselves functions of the angular coordinates $(\varphi, \theta)$. Consequently, the rate of change of unit vectors with respect to spherical coordinate variables must be also considered. Based on the definition of surface strain, the surface gradient of displacements can simply be extracted from the bulk displacement gradient projected onto the pit surface

$$\begin{aligned}
(\nabla_{\mathrm{S}}\boldsymbol{u})_{\varphi\varphi} &= \frac{1}{R}\left(u_R + \frac{\partial u_\varphi}{\partial\varphi}\right), \quad & (\nabla_{\mathrm{S}}\boldsymbol{u})_{\varphi\theta} &= \frac{1}{R}\left(\frac{1}{\sin\varphi}\frac{\partial u_\varphi}{\partial\theta} - \frac{\cos\varphi}{\sin\varphi}u_\theta\right),\\
(\nabla_{\mathrm{S}}\boldsymbol{u})_{\theta\varphi} &= \frac{1}{R}\frac{\partial u_\theta}{\partial\varphi}, & (\nabla_{\mathrm{S}}\boldsymbol{u})_{\theta\theta} &= \frac{1}{R\sin\varphi}\left(\frac{\partial u_\theta}{\partial\theta} + \cos\varphi u_\varphi + \sin\varphi u_R\right),\\
(\nabla_{\mathrm{S}}\boldsymbol{u})_{R\varphi} &= \frac{1}{R}\left(\frac{\partial u_R}{\partial\varphi} - u_\varphi\right), & (\nabla_{\mathrm{S}}\boldsymbol{u})_{R\theta} &= \frac{1}{R}\left(\frac{1}{\sin\varphi}\frac{\partial u_R}{\partial\theta} - u_\theta\right).
\end{aligned} \tag{18}$$

Plugging the above expressions into (15) produces the surface strain components

$$E_{\varphi\varphi} = \frac{u_R}{R} + \frac{1}{R}\frac{\partial u_\varphi}{\partial \varphi}, \quad E_{\theta\theta} = \frac{u_R}{R} + \frac{1}{R\sin\varphi}\frac{\partial u_\theta}{\partial \theta} + \frac{\cot\varphi u_\varphi}{R},$$
$$E_{\varphi\theta} = \tfrac{1}{2}\left(\frac{1}{R}\frac{\partial u_\theta}{\partial \varphi} - \frac{\cot\varphi u_\theta}{R} + \frac{1}{R\sin\varphi}\frac{\partial u_\varphi}{\partial \theta}\right). \tag{19}$$

By the use of (18) and (19) the surface constitutive law (16) can be reformulated directly in terms of surface displacements

$$\begin{aligned}
\Sigma_{\varphi\varphi} &= \frac{1}{R}\left\{(\lambda_0+2\mu_0)\left(u_R + \frac{\partial u_\varphi}{\partial \varphi}\right) + (\lambda_0+\tau_0)\left(u_R + \frac{\cos\varphi}{\sin\varphi}u_\varphi + \frac{1}{\sin\varphi}\frac{\partial u_\theta}{\partial \theta}\right)\right\},\\
\Sigma_{\varphi\theta} &= \frac{1}{R}\left\{\mu_0\left(\frac{1}{\sin\varphi}\frac{\partial u_\varphi}{\partial \theta} - \frac{\cos\varphi}{\sin\varphi}u_\theta\right) + (\mu_0-\tau_0)\frac{\partial u_\theta}{\partial \varphi}\right\},\\
\Sigma_{\theta\varphi} &= \frac{1}{R}\left\{\mu_0\frac{\partial u_\theta}{\partial \varphi} + (\mu_0-\tau_0)\left(\frac{1}{\sin\varphi}\frac{\partial u_\varphi}{\partial \theta} - \frac{\cos\varphi}{\sin\varphi}u_\theta\right)\right\},\\
\Sigma_{\theta\theta} &= \frac{1}{R}\left\{(\lambda_0+2\mu_0)\left(u_R + \frac{\cos\varphi}{\sin\varphi}u_\varphi + \frac{1}{\sin\varphi}\frac{\partial u_\theta}{\partial \theta}\right) + (\lambda_0+\tau_0)\left(u_R + \frac{\partial u_\varphi}{\partial \varphi}\right)\right\},\\
\Sigma_{R\varphi} &= \frac{\tau_0}{R}\left\{\frac{\partial u_R}{\partial \varphi} - u_\varphi\right\},\\
\Sigma_{R\theta} &= \frac{\tau_0}{R}\left\{\frac{1}{\sin\varphi}\frac{\partial u_R}{\partial \theta} - u_\theta\right\}.
\end{aligned} \tag{20}$$

The transform of the force balance condition (17) is less straightforward. Following Gurtin et al. [1998], explicit expressions of its three component equations can be developed with the help of a constant vector. In the present analysis, we have derived these expressions by first evaluating the surface gradient of the superficial surface stress tensor and subsequently contracting the second and third base vectors of the resultant third-order tensor. It should be noted that the surface gradient operator should be applied on the surface stress tensor from right to left [Malvern 1969], based on the argument in [Gurtin and Murdoch 1978]. Thus,

$$\begin{aligned}
\sigma_{RR}n_R &= \frac{1}{R}\left\{\frac{1}{\sin\varphi}\frac{\partial \Sigma_{R\theta}}{\partial \theta} + \frac{\partial \Sigma_{R\varphi}}{\partial \varphi} + \cot\varphi\,\Sigma_{R\varphi} - (\Sigma_{\theta\theta}+\Sigma_{\varphi\varphi})\right\} + T_R,\\
\sigma_{R\varphi}n_R &= \frac{1}{R}\left\{\frac{1}{\sin\varphi}\frac{\partial \Sigma_{\varphi\theta}}{\partial \theta} + \frac{\partial \Sigma_{\varphi\varphi}}{\partial \varphi} + \cot\varphi(\Sigma_{\varphi\varphi}-\Sigma_{\theta\theta}) + \Sigma_{R\varphi}\right\} + T_\varphi,\\
\sigma_{R\theta}n_R &= \frac{1}{R}\left\{\frac{1}{\sin\varphi}\frac{\partial \Sigma_{\theta\theta}}{\partial \theta} + \frac{\partial \Sigma_{\theta\varphi}}{\partial \varphi} + \cot\varphi(\Sigma_{\theta\varphi}+\Sigma_{\varphi\theta}) + \Sigma_{R\theta}\right\} + T_\theta,
\end{aligned} \tag{21}$$

where $\{T_R, T_\varphi, T_\theta\}$ denote the surface traction vector due to external loads. The above boundary conditions are valid for a general spherical free surface with unit normal vector $\boldsymbol{n} = \pm\boldsymbol{e}_R$. To proceed further, we could substitute (20) into (21) in order to develop general expressions of the surface divergence of the surface stresses in terms of displacements. It is these three boundary equations that couple the mechanics of a spherical free surface into the classical theory of elasticity for the abutting bulk solid. The development of their explicit expressions are straightforward yet quite tedious. Instead, we provide

a simplified version that is particularly tailored for the present axial torsion condition ($T_R = T_\varphi = 0$). In view of (5), it becomes obvious that only the last equation of (21) is nontrivial,

$$-\sigma_{R\theta} = (\nabla_S \cdot \Sigma)_\theta + T_\theta. \tag{22}$$

In this condition, $T_\theta$ now represents the distributed shear traction due to the external torque. The combination of equations (20) and (21) results in

$$(\nabla_S \cdot \Sigma)_\theta = -\frac{2\tau_0}{R^2}u_\theta + \frac{\mu_0}{R^2}\left(\frac{\partial^2 u_\theta}{\partial\varphi^2} + \frac{\cos\varphi}{\sin\varphi}\frac{\partial u_\theta}{\partial\varphi} - \frac{\cos^2\varphi}{\sin^2\varphi}u_\theta + u_\theta\right). \tag{23}$$

Furthermore, the change of the polar angular variable $\varphi$ to $\mu = \cos[\varphi]$ transforms the above equation to

$$(\nabla_S \cdot \Sigma)_\theta = -\frac{2\tau_0}{R^2}u_\theta + \frac{\mu_0}{R^2}\left((1-\mu^2)\frac{\partial^2 u_\theta}{\partial\mu^2} - 2\mu\frac{\partial u_\theta}{\partial\mu} + \frac{1-2\mu^2}{1-\mu^2}u_\theta\right). \tag{24}$$

Substituting the hoop displacement $u_\theta$ from (5) into the above relation and noting the harmonic property of the displacement potential $\lambda_3$,

$$\nabla^2\lambda_3 = \frac{\partial^2\lambda_3}{\partial R^2} + \frac{2}{R}\frac{\partial\lambda_3}{\partial R} + \frac{(1-\mu^2)}{R^2}\frac{\partial^2\lambda_3}{\partial\mu^2} - \frac{2\mu}{R^2}\frac{\partial\lambda_3}{\partial\mu}. \tag{25}$$

We may recast (24) in the form

$$\begin{aligned}(\nabla_S \cdot \Sigma)_\theta = {}& \frac{\tau_0}{2GR}\frac{2\sqrt{1-\mu^2}}{R^2}\left\{R\frac{\partial\lambda_3}{\partial R} - \mu\frac{\partial\lambda_3}{\partial\mu}\right\} \\ & - \frac{\mu_0}{2GR}\frac{\sqrt{1-\mu^2}}{R^2}\left\{2R\frac{\partial\lambda_3}{\partial R} - 2R^2\frac{\partial^2\lambda_3}{\partial R^2} - R^3\frac{\partial^3\lambda_3}{\partial R^3} - \mu\left(2\frac{\partial\lambda_3}{\partial\mu} - R^2\frac{\partial^3\lambda_3}{\partial R^2\partial\mu}\right)\right\}.\end{aligned} \tag{26}$$

In view of the proposed form of $\lambda_3$ from (7) we arrive at

$$(\nabla_S \cdot \Sigma)_\theta = -G\sqrt{1-\mu^2}\sum_{n=0}^{\infty}\left\{A_n\frac{(2n(2n+3)\mu_0 + 2\tau_0)}{2aG}((2n+1)P_{2n}[\mu] + \mu P'_{2n}[\mu])\right\}. \tag{27}$$

Eventually, by the use of (12) and (13) the surface divergence of the surface stress tensor is given by

$$(\nabla_S \cdot \Sigma)_\theta = \frac{G}{2}\sum_{n=0}^{\infty}\left\{A_n(2n(2n+3)\mu_0' + 2\tau_0')P^1_{2n+1}[\mu]\right\}, \tag{28}$$

where $\mu_0' = \mu_0/aG$ and $\tau_0' = \tau_0/aG$ are two intrinsic dimensionless parameters that characterize the strength of the hemispherical pit surface. It is worth noting that the other surface Lamé constant, $\lambda_0$, turns out to be irrelevant to the present axial-symmetric torsion problem.

Next, we substitute the shear stress $\sigma_{R\theta}$ from (11) and the surface divergence component $(\nabla_S \cdot \Sigma)_\theta$ from (28) into the nonclassical boundary condition (22)

$$\tfrac{1}{2}G\sum_{n=0}^{\infty}A_n((2n+3)(2n\mu_0' + 1) + 2\tau_0')P^1_{2n+1}[\mu] = -T_\theta[\mu]. \tag{29}$$

Since for each $m$, the associated Legendre functions $P_n^m$ of different $n$ are orthogonal and form a complete basis, thus it is possible to perform the series expansion

$$T_\theta[\mu] = \sum_{n=0}^{\infty} f_n P_{2n+1}^1[\mu], \tag{30}$$

where the coefficients $f_n$ are found by multiplying the series by $P_{2m+1}^1[\mu]$ and integrating term by term in the interval $\mu \in [0, 1]$. Using the orthogonality property of the associated Legendre functions

$$\int_{-1}^{1} P_{2n+1}^1[\mu] P_{2m+1}^1[\mu]\,\mathrm{d}\mu = \frac{2(2n+1)(2n+2)}{4n+3}\delta_{nm}, \tag{31}$$

and the parity relation

$$P_{2n+1}^1[-\mu] = P_{2n+1}^1[\mu], \tag{32}$$

we obtain

$$\int_{0}^{1} P_{2n+1}^1[\mu] P_{2m+1}^1[\mu]\,\mathrm{d}\mu = \frac{(2n+1)(2n+2)}{4n+3}\delta_{nm}. \tag{33}$$

As a result, it is derived that

$$f_n = \frac{4n+3}{(2n+1)(2n+2)} \int_{0}^{1} T_\theta[\mu] P_{2n+1}^1[\mu]\,\mathrm{d}\mu. \tag{34}$$

A simple comparison of (29) and (30) implies that the unknown coefficients $A_n$ can be connected to the expansion coefficients $f_n$ via

$$A_n = -\frac{2f_n}{G\{(2n+3)(2n\mu'_0+1)+2\tau'_0\}}. \tag{35}$$

Upon successful derivation of the unknown dimensionless coefficients $A_n$, the azimuthal displacement (10) and two shear stress components (11) can be evaluated as a function of the shear traction distribution $T_\theta$ and material parameters ($G$, $\nu$, $\mu'_0$ and $\tau'_0$).

## 3. Results and discussion

Clearly, the determination of the shear traction distribution $T_\theta$ from the applied net torque $T$ is an indeterminate problem. Different distributions might result in the same torque. Nevertheless, force equilibrium requires that

$$T = 2\pi a^3 \int_{0}^{1} T_\theta[\mu]\sqrt{1-\mu^2}\,\mathrm{d}\mu. \tag{36}$$

For a perfect elastic half-space without surface pits, a concentrated torque applied at the origin produces a shear stress distribution that is proportional to the $\sin\varphi$ [Hill 1966; Miyao et al. 1975]. Thus, we may assume

$$T_\theta[\mu] = T_0\sqrt{1-\mu^2}, \tag{37}$$

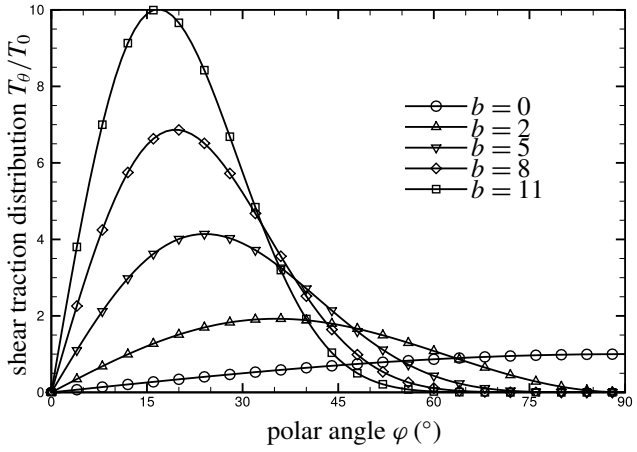


**Figure 2.** Distributions of five example shear tractions that result in the same torque load at the hemispherical pit surface ($\mu = \cos\varphi$).

where $T_0$ is the maximum shear traction evaluated at $\mu = \cos[\pi/2] = 0$. For the shear traction distribution (37), an expression that relates the maximum shear traction and the applied torque can be determined as

$$T_0 = \frac{3T}{4\pi a^3}. \tag{38}$$

For the general case of a pitted elastic half-space, the shear traction at the pit surface is treated as a distribution of the applied load and thus may have a different form. It was found that for an arbitrary nonnegative integer $b$, the shear traction distribution

$$T_\theta[\mu] = (T_0/3)(3 + 4b + b^2)\mu^b\sqrt{1-\mu^2}, \tag{39}$$

will result in the exact same torque as that of the fundamental distribution form (37). A few example distributions are

$$T_\theta[\mu] = \begin{cases} T_0\sqrt{1-\mu^2}, & b = 0, \\ 5T_0\mu^2\sqrt{1-\mu^2}, & b = 2, \\ 16T_0\mu^5\sqrt{1-\mu^2}, & b = 5, \\ 33T_0\mu^8\sqrt{1-\mu^2}, & b = 8, \\ 56T_0\mu^{11}\sqrt{1-\mu^2}, & b = 11. \end{cases} \tag{40}$$

For comparison purposes, the distributions of these five shear tractions are shown in Figure 2. It can be seen that the maximum value of the traction function transfers from the pit rim toward the hemispherical pit pole as $b$ increases.

Replacing $T_\theta[\mu]$ under the integral sign in (34) with the proposed shear traction distribution (39) and noticing the definite integral [Gradshteyn and Ryzhik 2014]

$$\int_0^1 \mu^b(1-\mu^2)^{m/2} P_\nu{}^m[\mu]\,\mathrm{d}\mu = \frac{(-1)^m 2^{-m-1}\Gamma\left[\frac{1}{2}+\frac{1}{2}b\right]\Gamma\left[1+\frac{1}{2}b\right]\Gamma[1+m+\nu]}{\Gamma[1-m+\nu]\Gamma\left[1+\frac{1}{2}b+\frac{1}{2}m-\frac{1}{2}\nu\right]\Gamma\left[\frac{3}{2}+\frac{1}{2}b+\frac{1}{2}m+\frac{1}{2}\nu\right]}, \tag{41}$$

it can be derived that

$$f_n = -\frac{T_0}{12}\frac{(3+4b+b^2)(4n+3)}{(2n+1)(2n+2)}\frac{\Gamma\left[\frac{1}{2}+\frac{1}{2}b\right]\Gamma\left[1+\frac{1}{2}b\right]\Gamma[2n+3]}{\Gamma[2n+1]\Gamma\left[1+\frac{1}{2}b-n\right]\Gamma\left[\frac{5}{2}+\frac{1}{2}b+n\right]}, \tag{42}$$

where $\Gamma[z] = (z-1)\Gamma[z-1]$ is referred to as the Gamma-factorial function [Arfken and Weber 2013]. The interesting result $\Gamma[1/2] = \sqrt{\pi}$ becomes very useful in the subsequent evaluation of the expansion coefficients $f_n$ in the Legendre series (30).

In view of (10), (11), (35) and (42), the semianalytical series representations of the solution have been successfully developed for the present problem. Prior to exploring solutions that must be represented by the Legendre series, let us examine a few simplified cases for which closed-form solutions are available. We first consider the fundamental distribution of shear tractions (37). We observe that for this case $T_\theta[\mu] = -T_0 P_1^1[\mu]$ and thus only the zeroth mode $f_0 = -T_0$ contributes to the series expansion. Evidently, (35) becomes

$$A_0 = -\frac{2f_0}{G(2\tau'_0+3)} = \frac{2T_0}{G(2\tau'_0+3)}. \tag{43}$$

A closed-form solution is now developed for the fundamental distribution of shear tractions

$$2Gu_\theta = -\frac{2T_0}{(2\tau'_0+3)}\frac{a^3}{R^2}P_1^1[\mu], \quad \sigma_{R\theta} = \frac{3T_0}{(2\tau'_0+3)}\frac{a^3}{R^3}P_1^1[\mu], \quad \sigma_{\varphi\theta} = 0. \tag{44}$$

Note that in this special case the stress component $\sigma_{\varphi\theta}$ vanishes.

The next case we examine is for $b = 2$ in (40). It is not hard to find that only two terms in the series expansion (30) are required since

$$T_\theta[\mu] = 5T_0\mu^2\sqrt{1-\mu^2} = f_0 P_1^1[\mu] + f_1 P_3^1[\mu], \tag{45}$$

where the two coefficients required in the expansion are given by $f_0 = -T_0$ and $f_1 = -2T_0/3$. As a result, (35) results in

$$A_0 = \frac{2T_0}{G(2\tau'_0+3)}, \quad A_1 = \frac{4T_0}{3G(10\mu'_0+2\tau'_0+5)}. \tag{46}$$

Similar to the case of fundamental traction distribution, closed-form displacements and stresses can now be identified as

$$\begin{aligned}
2Gu_\theta &= -\frac{2T_0}{(2\tau'_0+3)}\frac{a^3}{R^2}P_1^1[\mu] - \frac{4T_0}{3(10\mu'_0+2\tau'_0+5)}\frac{a^5}{R^4}P_3^1[\mu],\\
\sigma_{R\theta} &= \frac{3T_0}{(2\tau'_0+3)}\frac{a^3}{R^3}P_1^1[\mu] + \frac{10T_0}{3(10\mu'_0+2\tau'_0+5)}\frac{a^5}{R^5}P_3^1[\mu],\\
\sigma_{\varphi\theta} &= -\frac{2T_0}{3(10\mu'_0+2\tau'_0+5)}\frac{a^5}{R^5}P_3^2[\mu].
\end{aligned} \tag{47}$$

The availability of closed-form solutions is not an accident. As a matter of fact, the expansion coefficients $f_n$ are truncated by $n < 1 + b/2$ for a nonnegative even integer $b$ since $\Gamma[z]$ has simple poles at $z = 0, -1, -2, -3, -4, \ldots$. Such behavior is solely due to $\Gamma[1 + b/2 - n]$ in the denominator of (42). Thus, for a $b$ even and equal to $2s$, where $s$ is a positive integer, the shear traction distribution can be

represented by a truncated Legendre series expansion. Only the first $s+1$ terms are required in (30), e.g., $s=4$ for the fourth case ($b=8$) in (40). In this case, the closed-form displacements and stresses are given by

$$\begin{aligned}
2Gu_\theta &= -\frac{2T_0}{(2\tau'_0+3)}\frac{a^3}{R^2}P_1^1[\mu] - \frac{112T_0}{39(10\mu'_0+2\tau'_0+5)}\frac{a^5}{R^4}P_3^1[\mu] \\
&\quad - \frac{352T_0}{195(28\mu'_0+2\tau'_0+7)}\frac{a^7}{R^6}P_5^1[\mu] - \frac{128T_0}{221(54\mu'_0+2\tau'_0+9)}\frac{a^9}{R^8}P_7^1[\mu] \\
&\quad - \frac{256T_0}{3315(88\mu'_0+2\tau'_0+11)}\frac{a^{11}}{R^{10}}P_9^1[\mu], \\
\sigma_{R\theta} &= \frac{3T_0}{(2\tau'_0+3)}\frac{a^3}{R^3}P_1^1[\mu] + \frac{280T_0}{39(10\mu'_0+2\tau'_0+5)}\frac{a^5}{R^5}P_3^1[\mu] \\
&\quad + \frac{1232T_0}{195(28\mu'_0+2\tau'_0+7)}\frac{a^7}{R^7}P_5^1[\mu] + \frac{576T_0}{221(54\mu'_0+2\tau'_0+9)}\frac{a^9}{R^9}P_7^1[\mu] \\
&\quad + \frac{1408T_0}{3315(88\mu'_0+2\tau'_0+11)}\frac{a^{11}}{R^{11}}P_9^1[\mu], \\
\sigma_{\varphi\theta} &= -\frac{56T_0}{39(10\mu'_0+2\tau'_0+5)}\frac{a^5}{R^5}P_3^2[\mu] - \frac{176T_0}{195(28\mu'_0+2\tau'_0+7)}\frac{a^7}{R^7}P_5^2[\mu] \\
&\quad - \frac{64T_0}{221(54\mu'_0+2\tau'_0+9)}\frac{a^9}{R^9}P_7^2[\mu] - \frac{128T_0}{3315(88\mu'_0+2\tau'_0+11)}\frac{a^{11}}{R^{11}}P_9^2[\mu],
\end{aligned} \tag{48}$$

It is worth noting that if $b$ is odd, the coefficients of the Legendre series expansion $f_n$ are well defined for every $n$. Fortunately, the coefficient of expansion $f_n$ behaves as a strong decaying function of $n$ and thus it is possible to truncate the series with a desired accuracy.

In the remainder of this section, parametric study was employed to facilitate the investigation of surface effects. In view of (35), (44), (47) and (48) it can be seen that the influence of surface mechanics becomes important when $\tau'_0$ and $\mu'_0$ approach the order of magnitudes of unity and one tenth, respectively. For smaller magnitudes of $\tau'_0$ and $\mu'_0$, the incorporation of surface mechanics introduces inappreciable modifications to the classical solution. The magnitude of both the residual surface stress $\tau_0$ and the surface shear modulus $\mu_0$ of typical crystalline metal materials is 1 N/m [Mi et al. 2008] whereas that of their bulk modulus is $\sim 10^{10}$ Pa [Gere and Goodno 2009]. As a result, the order of magnitude of the pit radius $a$ must be nearly as large as the subnanoscale to cause noticeable surface effects. This is because only the deformation-dependent component of the surface constitutive law (17) can be accommodated in a torsion problem. This scenario is in sharp contrast with that of the dilatational deformation mode in which significant surface influence can still be observed at much larger characteristic length scales [He and Li 2006; Mi and Kouris 2014b].

Nevertheless, the story could be quite different for soft materials in which the relative magnitude between surface elastic parameters and bulk shear modulus increases remarkably. As intuition could expect, soft materials possess much smaller bulk shear modulus in magnitude. For example, the shear modulus of rubber falls in the interval of $0.2-1$ MPa [Gere and Goodno 2009]. More strikingly, the shear modulus of gelatin is in the order of tens of kPa ($\sim 10^4$ N/m$^2$). Specimens made by these soft materials

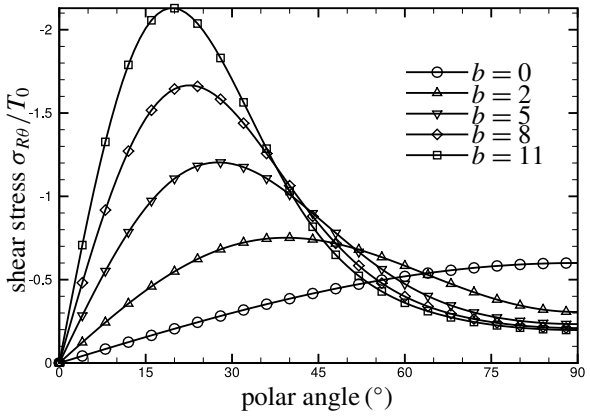


**Figure 3.** The distribution of normalized shear stress ($\sigma_{R\theta}/T_0$) as a function of the polar angle ($\varphi$) at the hemispherical pit surface ($R = a$). Numerical values of the two intrinsic dimensionless parameters are taken as $\mu_0' = \tau_0' = 1$.

stay fairly linearly elastic for strains below 10% of such a level of shear modulus, while the Young's modulus ranges from a few kPa to a few hundred kPa [Markidou et al. 2005]. The shear modulus of gelatin gels fluctuates with a few factors including concentration, preparation procedure of testing samples and temperatures at which the measurement was performed.

Little work has been done on the estimation of the surface mechanical properties for soft materials compared to that of crystalline systems. Bialopiotrowicz and Janczuk [2002] managed to employ the method of contact angle measurement to investigate the wetting characteristics of gelatin films and a number of liquids. For those probe liquids with known energy components, the surface free energy of a gelatin film is able to be determined. Experimental measurements demonstrate that the surface free energy of gelatin films with concentrations ranging $0.005 - 100$ mg/mL is in the magnitude of a few tens of mJ/m$^2$. Based on the force equilibrium, Weijs et al. [2014] developed a microscopic model that correlates the interface stress and interface energy for an interface separating a liquid and an amorphous soft solid. Although the quantitative behavior of their model is governed by the Poisson's ratio of the interfacial region, the interface stress and interface energy share the same order of magnitude. Furthermore, the definition of elastic modulus [Gumbsch and Daw 1991; Mi et al. 2008] explains that interface energy, interface stress and interface elastic moduli are all about the same order of magnitude ($\sim 10^{-2}$ N/m).

To summarize the dimension analysis up to this point, for soft materials such as gelatin gels the effects of surface mechanics become noticeable and even significant when the characteristic length goes down to the microscale ($a \leq 10^{-6}$ m). At such a length scale, those two intrinsic dimensionless parameters are both comparable to unity ($\mu_0' = \mu_0/aG \sim 1$ and $\tau_0' = \tau_0/aG \sim 1$) and thus the model of surface mechanics starts to participate in the mechanics and physics of the concerned material systems. Of course, for rubber-like soft materials, a smaller length scale is preferred for highlighting the surface effects.

Figure 3 shows the distributions of the normalized shear stress $\sigma_{R\theta}/T_0$ at the hemispherical pit surface resulting from the five example shear tractions emphasized in Figure 2. Undoubtedly, these shear stress

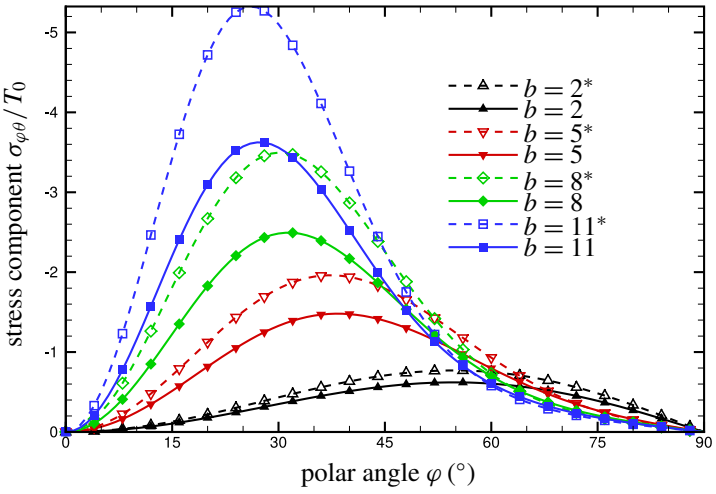


**Figure 4.** The distribution of normalized stress component ($\sigma_{\varphi\theta}/T_0$) as a function of the polar angle ($\varphi$) at the hemispherical pit surface ($R = a$). Numerical values of the two intrinsic dimensionless parameters are taken as $\mu_0' = \tau_0' = 0.1$. For comparison, the corresponding classical solutions ($\mu_0' = \tau_0' = 0$) are also shown, indicated by $^*$.

distributions would exactly recover to the shear tractions within the framework of the classical theory of elasticity. Nonetheless, the model of surface mechanics ($\mu_0' = \tau_0' = 1$) has reduced the maximum shear stress by more than 40% for all cases. The strength of surface mechanics increases monotonically with $b$. For $b = 11$, the maximum shear stress becomes less than one fourth of its classical counterpart. Close examination reveals that the value of the polar angle coordinate $\varphi$ at which the maximum shear stress takes place is now closer to the vertex $A$ of the hemispherical pit. Furthermore, the stress level at the pit perimeter ($\varphi = 90°$) seems to converge to a limit value ($\sigma_{R\varphi} \sim -0.2T_0$) as the parameter $b$ increases. This behavior is clearly not observed in the classical solutions, cf. Figure 2.

The comparison of Figures 2 and 3 makes it clear that the parameter combination $\mu_0' = \tau_0' = 1$ represents a fairly strong effect of surface mechanics. To better illustrate the effects of surface mechanics, we now adjust these parameters to $\mu_0' = \tau_0' = 0.1$. The curves in Figure 4 show the distributions of the normalized stress component $\sigma_{\varphi\theta}/T_0$ at the pit surface for four traction distributions ($b = 2, 5, 8$ and 11). Note that this stress component vanishes for the case of $b = 0$, see (44). Both the curves with and without the model of surface mechanics are plotted for the purpose of comparison. For both groups, $\sigma_{\varphi\theta}$ becomes zero at the pit vertex $A$ and the pit perimeter $B$, defined in Figure 1. For a given value of $b$, the maximum stress occurs at the same place for both the classical and corrected solution. These places are $\varphi = 55, 38, 31$ and 27 degrees for $b = 2, 5, 8$ and 11, respectively. We expect that the value of $\varphi$ at which the stress extremities take place will converge to a specific value as $b$ continues to increase. The strength of surface mechanics depends on how the shear tractions distribute — the larger the value of $b$, the stronger the surface effects become.

Figure 5 shows the distributions of the dimensionless displacement $2Gu_\theta/T_0/a$ at the pit surface for the five example traction loads. These curves share similar distribution characteristics as those of

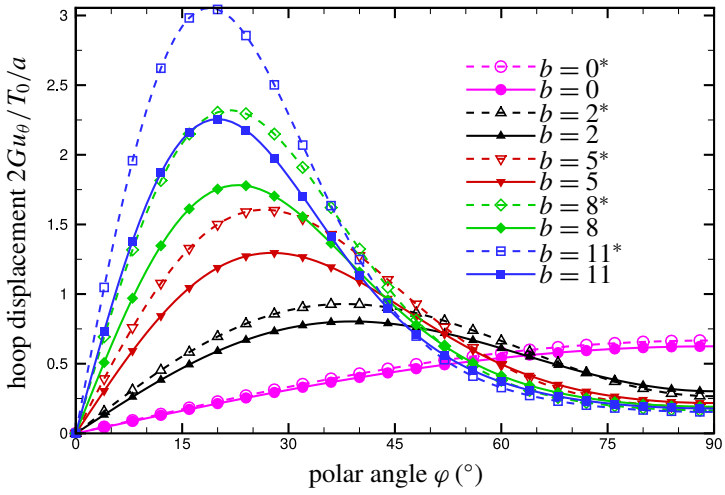


**Figure 5.** The distribution of normalized hoop component ($2Gu_\theta/T_0/a$) as a function of the polar angle ($\varphi$) at the hemispherical pit surface ($R = a$). Numerical values of the two intrinsic dimensionless parameters are taken as $\mu_0' = \tau_0' = 0.1$. For comparison, the corresponding classical solutions ($\mu_0' = \tau_0' = 0$) are also shown, indicated by $^*$.

the shear stress $\sigma_{R\theta}$. Displacement extremities roughly occur at the same locations. Once again, the significance of surface mechanics depends on loading mode of surface tractions. For $b = 2, 5, 8$ and 11, crossovers are observed between the classical and perturbed curves belonging to the same traction mode. The coordinates of these intersections behave as functions of the loading mode — the larger the parameter $b$, the farther the crossover deviates from the pit perimeter.

To investigate the range of the elastic field resulting from the surface tractions applied at the pit surface, we further performed numerical experiments to evaluate the displacements and stresses on a couple of concentric hemispherical coordinate surfaces. Shown in Figure 6 is the distribution of the normalized shear stress $\sigma_{R\theta}/T_0$ for three surface traction loads ($b = 0$, 5 and 11) at two radial distances ($R = 1.5a$ and $R = 2a$). The classical solutions for which $\mu_0' = \tau_0' = 0$ are also plotted for each of the six cases. Although the variation characteristics for an individual curve is quite similar to its corresponding counterpart at the pit surface, see Figures 2 and 3, the stress magnitude decays drastically as the radial coordinate increases. For example, the maximum stress for the case of $b = 11$ reduced more than nine tenths as the radial coordinate changes from $R = a$ to $R = 1.5a$. The rate of decay is slightly slower for the solution accounting for surface effects as the maximum stress decreased approximately two thirds. For both the classical and modified solutions, the traction loads applied at the pit surface on the plane boundary of an elastic half-space is a short-range force field since the resulting elastic field is completely localized and confined within a distance that is just a couple of multiples of the pit radius.

Numerical results shown in Figure 7 and Figure 8 further support the argument of a localized elastic field made above in which the normalized stress $\sigma_{\varphi\theta}/T_0$ and displacement component $2Gu_\theta/T_0/a$ are now plotted for the radial coordinates $R = 1.25a$ and $R = 1.5a$. It should be noted that Figure 7 only shows two modes of traction loads ($b = 5$ and 11) since $\sigma_{\varphi\theta}$ is identically zero for the fundamental

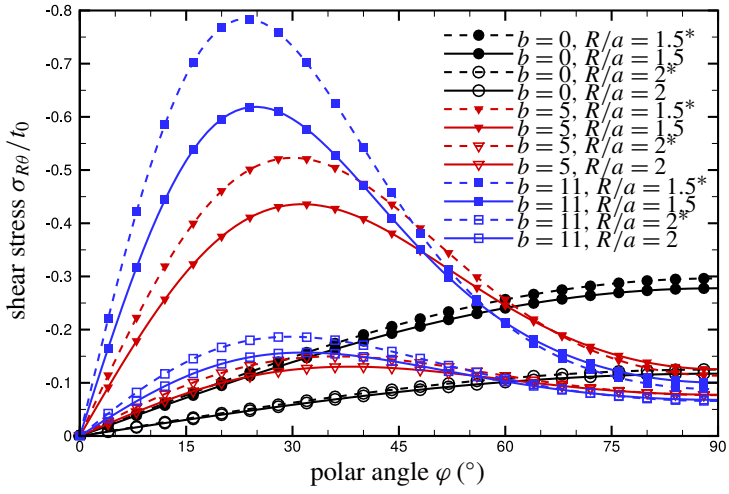


**Figure 6.** The distribution of normalized shear stress ($\sigma_{R\theta}/T_0$) as a function of the polar angle ($\varphi$) for two constant radial coordinates ($R = 1.5a$ and $2a$). Numerical values of the two intrinsic dimensionless parameters are taken as $\mu_0' = \tau_0' = 0.1$. For comparison, results due to three traction distributions ($b = 0$, 5 and 11) are plotted with the classical solutions indicated by $^*$.

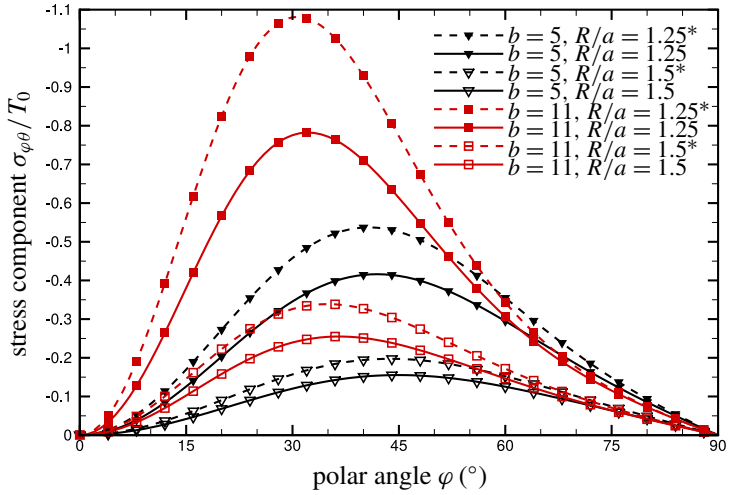


**Figure 7.** The distribution of normalized stress component ($\sigma_{\varphi\theta}/T_0$) as a function of the polar angle ($\varphi$) for two constant radial coordinates ($R = 1.25a$ and $1.5a$). Numerical values of the two intrinsic dimensionless parameters are taken as $\mu_0' = \tau_0' = 0.1$. For comparison, results due to two traction distributions ($b = 5$ and 11) are plotted with the classical solutions indicated by $^*$.

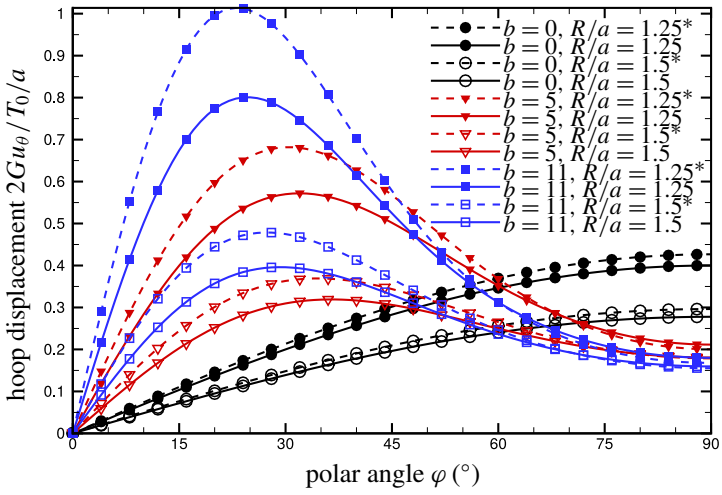


**Figure 8.** The distribution of normalized hoop displacement ($2Gu_\theta/T_0/a$) as a function of the polar angle ($\varphi$) for two constant radial coordinates ($R = 1.25a$ and $1.5a$). Numerical values of the two intrinsic dimensionless parameters are taken as $\mu_0' = \tau_0' = 0.1$. For comparison, results due to three traction distributions ($b = 0$, 5 and 11) are plotted with the classical solutions indicated by *.

traction distribution ($b = 0$). The trend of decay as a function of the radial coordinate is obvious for the stress $\sigma_{\varphi\theta}$ (Figure 7) and the displacement component $u_\theta$ (Figure 8). These elastic components become numerically negligible at a distance only a few radii away from the pit center.

## 4. Concluding remarks

In this paper, we analyzed in detail the axial-symmetric torsion problem of a nanoscale hemispherical pit on the plane boundary of a semi-infinite elastic solid. We considered a number of traction loads, see (39), that are proportional to the shear stress distribution on a hemispherical coordinate surface due to a concentrated torque applied on an intact half-space. Although all considered traction loads resulted in the exact same torque, displacement and stress distributions differ from one case to another, reflecting the indeterminate nature of the problem. Semianalytical solutions in the form of infinite series were successfully developed. Within the framework of Gurtin and Murdoch's theory of surface elasticity [1978], two intrinsic dimensionless parameters, $\mu_0' = \mu_0/Ga$ and $\tau_0' = \tau_0/Ga$, were formulated to account for the significance of the pit surface. The other surface Lamé parameter $\lambda_0$, which is indispensable to a torsionless problem, turns out to be irrelevant in the present analysis.

Dimension analysis carried out in the previous section suggests that the assumed model of a pit surface can reasonably be neglected for a metal substrate. The drastic difference between metals' surface and bulk elastic constants make the two dimensionless parameters comparable to unity only for picoscale pits. Nonetheless, for soft substrates, such as gelatin gels, the pit surface effects became a dominant factor that affected the resulting stress levels. To bring the model of surface mechanics into effect, we inferred that $\mu_0'$ and $\tau_0'$ should be at the order of magnitude of unity and one tenth, respectively — which is fairly

practical for a soft substrate [Białopiotrowicz and Jańczuk 2002; Weijs et al. 2014]. It can be further argued that the surface shear modulus $\mu_0$ is more important than the residual surface stress $\tau_0'$ in a torsion problem. This interpretation is in opposition to a dilatational problem in which the residual surface stress proves to be much more important than surface Lamé constants [Mi and Kouris 2014b]. The reason is due to the fact that the deformation-dependent component of the surface constitutive relation is not applicable in the torsion analysis. Numerical results prove that the parameter combination of $\mu_0' = \tau_0' = 0.1$ is strong enough to change both the magnitude and distribution of the classical solution when the model of surface mechanics is excluded.

We have based our calculations merely on nominal values of the two dimensionless parameters, $\mu_0'$ and $\tau_0'$. For a practical soft material, it is a challenge to determine accurate values of surface and bulk elastic parameters. Considering what has been done for metal systems [Gumbsch and Daw 1991; Shenoy 2005; Mi et al. 2008], this could be one future line of research. Another possibility is to extend the static problem to investigate the coupling effects of surface mechanics and dynamic loading.

## Acknowledgements

This work was supported by the Natural Science Foundation of Jiangsu Province (Grant no. BK20130597), the National Natural Science Foundation of China (Grant no. 11472079), and the Project Sponsored by the Scientific Research Foundation for the Returned Overseas Chinese Scholars, State Education Ministry.

## References

[Arfken and Weber 2013] G. B. Arfken and H. J. Weber, *Mathematical methods for physicists*, 7th ed., Harcourt/Academic Press, Burlington, Massachusetts, 2013.

[Barber 2010] J. Barber, *Elasticity*, 3rd ed., Solid Mechanics and Its Applications, Springer, New York, 2010.

[Białopiotrowicz and Jańczuk 2002] T. Białopiotrowicz and B. Jańczuk, "Surface properties of gelatin films", *Langmuir* **18**:24 (2002), 9462–9468.

[Chadwick and Johnson 1971] P. Chadwick and A. F. Johnson, "High-frequency torsional oscillations of a rigid inclusion embedded in an elastic solid", *Q. J. Mech. Appl. Math.* **24**:1 (1971), 105–114.

[Eringen 1957] A. C. Eringen, "Elasto-dynamic problem concerning the spherical cavity", *Q. J. Mech. Appl. Math.* **10** (1957), 257–270.

[Gere and Goodno 2009] J. M. Gere and B. J. Goodno, *Mechanics of materials*, 7th ed., Cengage Learning, Toronto, 2009.

[Gradshteyn and Ryzhik 2014] I. S. Gradshteyn and I. M. Ryzhik, *Table of integrals, series, and products*, 8th ed., edited by D. Zwillinger and V. Moll, Elsevier Academic Press, Boston, 2014.

[Gumbsch and Daw 1991] P. Gumbsch and M. S. Daw, "Interface stresses and their effects on the elastic moduli of metallic multilayers", *Phys. Rev. B* **44** (1991), 3934–3938.

[Gurtin 1998] M. E. Gurtin, "A general theory of curved deformable interfaces in solids at equilibrium", *Philos. Mag. A* **78**:5 (1998), 1093–1109.

[Gurtin and Murdoch 1975] M. E. Gurtin and A. I. Murdoch, "A continuum theory of elastic material surfaces", *Arch. Rational Mech. Anal.* **57** (1975), 291–323.

[Gurtin and Murdoch 1978] M. E. Gurtin and A. I. Murdoch, "Surface stress in solids", *Int. J. Solids Struct.* **14**:6 (1978), 431–440.

[He and Li 2006] L. H. He and Z. R. Li, "Impact of surface stress on stress concentration", *Int. J. Solids Struct.* **43**:20 (2006), 6208–6219.

[Hill 1966] J. L. Hill, "Torsional-wave propagation from a rigid sphere semiembedded in an elastic half-space", *J. Acoust. Soc. Am.* **40**:2 (1966), 376–379.

[Kausel 2010] E. Kausel, "Early history of soil-structure interaction", *Soil Dyn. Earthq. Eng.* **30**:9 (2010), 822–832.

[Kushch et al. 2013] V. I. Kushch, S. G. Mogilevskaya, H. K. Stolarski, and S. L. Crouch, "Elastic fields and effective moduli of particulate nanocomposites with the Gurtin–Murdoch model of interfaces", *Int. J. Solids Struct.* **50**:7–8 (2013), 1141–1153.

[Malvern 1969] L. E. Malvern, *Introduction to the mechanics of a continuous medium*, Prentice-Hall, 1969.

[Markidou et al. 2005] A. Markidou, W. Y. Shih, and W.-H. Shih, "Soft-materials elastic and shear moduli measurement using piezoelectric cantilevers", *Rev. Sci. Instrum.* **76**:6 (2005).

[Mi and Kouris 2006] C. Mi and D. Kouris, "Nanoparticles under the influence of surface/interface elasticity", *J. Mech. Mater. Struct.* **1**:4 (2006), 763–791.

[Mi and Kouris 2013] C. Mi and D. Kouris, "Stress concentration around a nanovoid near the surface of an elastic half-space", *Int. J. Solids Struct.* **50**:18 (2013), 2737–2748.

[Mi and Kouris 2014a] C. Mi and D. Kouris, "Elastic disturbance due to a nanoparticle near a free surface", *Math. Mech. Solids* **19**:7 (2014), 868–881.

[Mi and Kouris 2014b] C. Mi and D. Kouris, "On the significance of coherent interface effects for embedded nanoparticles", *Math. Mech. Solids* **19**:4 (2014), 350–368.

[Mi and Kouris 2015] C. Mi and D. Kouris, "Surface mechanics implications for a nanovoided metallic thin-plate under uniform boundary loading", *Math. Mech. Solids* (2015).

[Mi et al. 2008] C. Mi, S. Jun, D. A. Kouris, and S. Y. Kim, "Atomistic calculations of interface elastic properties in noncoherent metallic bilayers", *Phys. Rev. B* **77** (2008), 075425.

[Mi et al. 2011] C. Mi, D. A. Buttry, P. Sharma, and D. A. Kouris, "Atomistic insights into dislocation-based mechanisms of void growth and coalescence", *J. Mech. Phys. Solids* **59**:9 (2011), 1858–1871.

[Miyao et al. 1975] S. Miyao, E. Tsuchida, H. Matsumoto, and I. Nakahara, "A semi-infinite body subjected to an impulsive torque on a hemispherical pit of a free surface", *B. JSME* **18**:123 (1975), 959–964.

[Mogilevskaya et al. 2008] S. G. Mogilevskaya, S. L. Crouch, and H. K. Stolarski, "Multiple interacting circular nano-inhomogeneities with surface/interface effects", *J. Mech. Phys. Solids* **56**:6 (2008), 2298–2327.

[Mogilevskaya et al. 2010] S. G. Mogilevskaya, S. L. Crouch, A. L. Grotta, and H. K. Stolarski, "The effects of surface elasticity and surface tension on the transverse overall elastic behavior of unidirectional nano-composites", *Compos. Sci. Technol.* **70**:3 (2010), 427–434.

[Osman and Rouainia 2012] A. S. Osman and M. Rouainia, "Dynamic response of an axially loaded rigid sphere embedded in a saturated poroelastic medium", *Arch. Appl. Mech.* **82**:3 (2012), 407–421.

[Reissner and Sagoci 1944] E. Reissner and H. F. Sagoci, "Forced torsional oscillations of an elastic half-space, I", *J. Appl. Phys.* **15** (1944), 652–654.

[Sharma et al. 2003] P. Sharma, S. Ganti, and N. Bhate, "Effect of surfaces on the size-dependent elastic state of nano-inhomogeneities", *Appl. Phys. Lett.* **82**:4 (2003), 535–537.

[Shenoy 2005] V. B. Shenoy, "Atomistic calculations of elastic properties of metallic fcc crystal surfaces", *Phys. Rev. B* **71** (2005), 094104.

[Steigmann and Ogden 1999] D. J. Steigmann and R. W. Ogden, "Elastic surface-substrate interactions", *R. Soc. Lond. Proc. Ser. A Math. Phys. Eng. Sci.* **455**:1982 (1999), 437–474.

[Streitz et al. 1994] F. H. Streitz, R. C. Cammarata, and K. Sieradzki, "Surface-stress effects on elastic properties, I: Thin metal films", *Phys. Rev. B* **49** (1994), 10699–10706.

[Todhunter and Pearson 2010] I. Todhunter and K. Pearson, *A history of the theory of elasticity and of the strength of materials: from Galilei to the present time*, vol. 2, Kessinger, 2010.

[Wang et al. 2011] J. Wang, Z. Huang, H. Duan, S. Yu, X. Feng, G. Wang, W. Zhang, and T. Wang, "Surface stress effect in mechanics of nanostructured materials", *Acta Mech. Solida Sin.* **24**:1 (2011), 52–82.

[Weijs et al. 2014] J. H. Weijs, J. H. Snoeijer, and B. Andreotti, "Capillarity of soft amorphous solids: a microscopic model for surface stress", *Phys. Rev. E* **89** (2014), 042408.

[Williams 1971] W. E. Williams, "Slow torsional oscillations of a rigid inclusion in an elastic medium", *Q. J. Mech. Appl. Math.* **24**:1 (1971), 99–104.

[Young and Budynas 2002] W. C. Young and R. G. Budynas, *Roark's formulas for stress and strain*, 7th ed., McGraw–Hill, New York, 2002.

[Zakout et al. 1999] U. Zakout, Z. Akkas, and G. E. Tupholme, "Transient response of an infinite elastic medium containing a spherical cavity subjected to torsion", *J. Appl. Mech.* **67**:2 (1999), 282–287.

Received 31 Mar 2016. Revised 12 Aug 2016. Accepted 13 Aug 2016.

CHANGWEN MI: mi@seu.edu.cn
*Jiangsu Key Laboratory of Engineering Mechanics, School of Civil Engineering, Southeast University, 2 Sipailou Street, Nanjing, 210096, China*

ZHONGWEI SUN: 2318125756@qq.com
*Jiangsu Key Laboratory of Engineering Mechanics, School of Civil Engineering, Southeast University, 2 Sipailou Street, Nanjing, 210096, China*

DEMITRIS KOURIS: Demitris.Kouris@sdsmt.edu
*Office of the Provost, South Dakota School of Mines & Technology, 501 East St. Joseph Street, Rapid City, SD 57701, United States*

# JOURNAL OF MECHANICS OF MATERIALS AND STRUCTURES

msp.org/jomms

Founded by Charles R. Steele and Marie-Louise Steele



**EDITORIAL BOARD**

| | |
|---|---|
| ADAIR R. AGUIAR | University of São Paulo at São Carlos, Brazil |
| KATIA BERTOLDI | Harvard University, USA |
| DAVIDE BIGONI | University of Trento, Italy |
| YIBIN FU | Keele University, UK |
| IWONA JASIUK | University of Illinois at Urbana-Champaign, USA |
| C. W. LIM | City University of Hong Kong |
| THOMAS J. PENCE | Michigan State University, USA |
| GIANNI ROYER-CARFAGNI | Università degli studi di Parma, Italy |
| DAVID STEIGMANN | University of California at Berkeley, USA |
| PAUL STEINMANN | Friedrich-Alexander-Universität Erlangen-Nürnberg, Germany |

**ADVISORY BOARD**

| | |
|---|---|
| J. P. CARTER | University of Sydney, Australia |
| D. H. HODGES | Georgia Institute of Technology, USA |
| J. HUTCHINSON | Harvard University, USA |
| D. PAMPLONA | Universidade Católica do Rio de Janeiro, Brazil |
| M. B. RUBIN | Technion, Haifa, Israel |

**PRODUCTION** production@msp.org

SILVIO LEVY Scientific Editor


Cover photo: Wikimedia Commons


See msp.org/jomms for submission guidelines.

JoMMS (ISSN 1559-3959) at Mathematical Sciences Publishers, 798 Evans Hall #6840, c/o University of California, Berkeley, CA 94720-3840, is published in 10 issues a year. The subscription price for 2016 is US $575/year for the electronic version, and $735/year (+$60, if shipping outside the US) for print and electronic. Subscriptions, requests for back issues, and changes of address should be sent to MSP.

JoMMS peer-review and production is managed by EditFLOW® from Mathematical Sciences Publishers.

PUBLISHED BY

mathematical sciences publishers

nonprofit scientific publishing

http://msp.org/



© 2016 Mathematical Sciences Publishers

Journal of Mechanics of Materials and Structures

Volume 11, No. 5 December 2016



1559-3959(2016)11:5;1-4